



**HAL**  
open science

## Molecule-based microelectromechanical sensors

Matias Imanol Urdampilleta, Cédric Ayela, Pierre-Henri Ducrot, Daniel Rosario-Amorin, Abhishake Mondal, Mathieu Rouzières, Pierre Dechambenoit, Corine Mathonière, Fabrice Mathieu, Isabelle Dufour, et al.

► **To cite this version:**

Matias Imanol Urdampilleta, Cédric Ayela, Pierre-Henri Ducrot, Daniel Rosario-Amorin, Abhishake Mondal, et al.. Molecule-based microelectromechanical sensors. Scientific Reports, 2018, 8, pp.8016. 10.1038/s41598-018-26076-2 . hal-01793761

**HAL Id: hal-01793761**

**<https://hal.science/hal-01793761v1>**

Submitted on 26 Jun 2019

**HAL** is a multi-disciplinary open access archive for the deposit and dissemination of scientific research documents, whether they are published or not. The documents may come from teaching and research institutions in France or abroad, or from public or private research centers.

L'archive ouverte pluridisciplinaire **HAL**, est destinée au dépôt et à la diffusion de documents scientifiques de niveau recherche, publiés ou non, émanant des établissements d'enseignement et de recherche français ou étrangers, des laboratoires publics ou privés.

# SCIENTIFIC REPORTS



OPEN

## Molecule-based microelectromechanical sensors

Matias Urdampilleta<sup>1,2</sup>, Cedric Ayela<sup>3,4,5</sup>, Pierre-Henri Ducrot<sup>3,4,5</sup>, Daniel Rosario-Amorin<sup>1,2</sup>, Abhishake Mondal<sup>1,2</sup>, Mathieu Rouzières<sup>1,2</sup>, Pierre Dechambenoit<sup>1,2</sup>, Corine Mathonière<sup>6,7</sup>, Fabrice Mathieu<sup>8</sup>, Isabelle Dufour<sup>3,4,5</sup> & Rodolphe Clérac<sup>1,2</sup> 

Received: 7 September 2017

Accepted: 23 April 2018

Published online: 22 May 2018

Incorporating functional molecules into sensor devices is an emerging area in molecular electronics that aims at exploiting the sensitivity of different molecules to their environment and turning it into an electrical signal. Among the emergent and integrated sensors, microelectromechanical systems (MEMS) are promising for their extreme sensitivity to mechanical events. However, to bring new functions to these devices, the functionalization of their surface with molecules is required. Herein, we present original electronic devices made of an organic microelectromechanical resonator functionalized with switchable magnetic molecules. The change of their mechanical properties and geometry induced by the switching of their magnetic state at a molecular level alters the device's dynamical behavior, resulting in a change of the resonance frequency. We demonstrate that these devices can be operated to sense light or thermal excitation. Moreover, thanks to the collective interaction of the switchable molecules, the device behaves as a non-volatile memory. Our results open up broad prospects of new flexible photo- and thermo-active hybrid devices for molecule-based data storage and sensors.

The development of molecule-based electronic devices for sensing or computation requires the synthesis of new materials and the fabrication of new architectures. As a result, switchable molecules, which can be turned into two different states using an external stimulus, have been thoroughly investigated during the last decade<sup>1–4</sup>. Their switching can be activated using a wide range of external excitations such as photons<sup>5</sup>, tunneling electrons<sup>6</sup>, chemical species<sup>7</sup>, or temperature<sup>8</sup>. Among the large variety of molecular switches, magnetic molecules have attracted a lot of interest as they combine interesting magnetic, electronic and mechanical properties<sup>9</sup> and can be, in certain cases, photoactivated<sup>10,11</sup>. These magnetic molecular switches (MMSs)<sup>12</sup> possess two accessible states with high-spin (HS) and low-spin (LS) configurations. The switching between these two states can be induced either by a change in the spin configuration of a metal center (e.g. spin crossover compounds)<sup>9–12</sup> or by the transfer of one electron from one metal site to another (e.g. electron transfer molecules)<sup>13,14</sup>. The HS/LS conversion is commonly driven by a competition between the enthalpy and the entropy of the system. Thus, a change of the molecular spin is observed as a function of the temperature with the LS state being favorable below the crossover temperature. Remarkably, once in their LS state, the MMSs can be photo-switched in their HS state<sup>9–14</sup>.

Interestingly, the HS/LS switching involves an electronic redistribution between the non-bonding  $t_{2g}$  and bonding  $e_g$  orbitals of the metal ions, leading to a change of the molecule geometry and volume, as schematized in Fig. 1a. Therefore, this effect leads to a change of the mechanical properties of the switchable material. Recently, it has been proposed to exploit these properties by integrating MMSs in a free-standing mechanical system<sup>15–17</sup>. An alternative experimental approach consists in using an inorganic microelectromechanical system (MEMS) functionalized with switchable magnetic molecules for which the change of mechanical properties affects the resonance frequency of the device<sup>18,19</sup>. Another interesting and powerful approach to expand the application capability of the molecular switches is the use of organic MEMS<sup>20</sup>. In this case, large variations of the organic MEMS resonance could be observed when a surface stress is generated by the volume change of the MMSs. This idea has been experimentally demonstrated here. We have measured unprecedentedly large resonance frequency shifts of the hybrid device when the molecules experience a switching, either induced by thermal or optical excitations.

<sup>1</sup>CNRS, CRPP, UMR 5031, 33600, Pessac, France. <sup>2</sup>University Bordeaux, CRPP, UMR 5031, 33600, Pessac, France.

<sup>3</sup>University Bordeaux, IMS, UMR 5218, F-33405, Talence, France. <sup>4</sup>CNRS, IMS, UMR 5218, F-33405, Talence, France.

<sup>5</sup>Bordeaux INP, IMS, UMR 5218, F-33405, Talence, France. <sup>6</sup>CNRS, ICMCB, UMR 5026, 33608, Pessac Cedex, France.

<sup>7</sup>University Bordeaux, ICMCB, UMR 5026, 33600, Pessac, France. <sup>8</sup>LAAS, CNRS et Université de Toulouse, INSA, UPS, F-31077, Toulouse, France. Correspondence and requests for materials should be addressed to M.U. (email: [matias.urdampilleta@neel.cnrs.fr](mailto:matias.urdampilleta@neel.cnrs.fr)) or C.A. (email: [cedric.ayela@ims-bordeaux.fr](mailto:cedric.ayela@ims-bordeaux.fr)) or R.C. (email: [clerac@crpp-bordeaux.cnrs.fr](mailto:clerac@crpp-bordeaux.cnrs.fr))

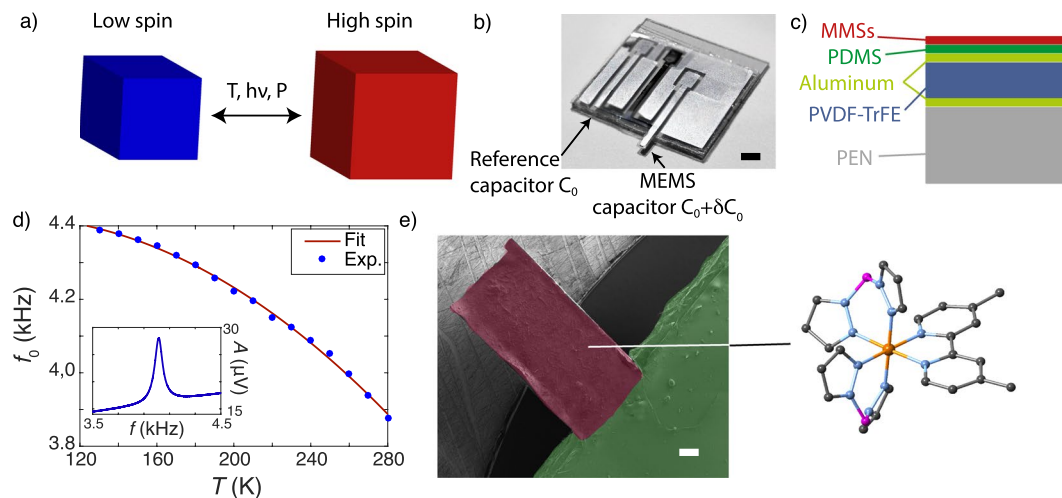


**Figure 1.** A molecule-based MEMS. **(a)** Scheme illustrating that the magnetic switching can be activated in a MMS using different stimuli: temperature, light or pressure. The change of magnetic state is accompanied by a change of the molecule volume. **(b)** View of a chip implemented with the organic piezoelectric microelectromechanical system and the reference structure. Scale bar is 2 mm. **(c)** Scheme of the cut view of the MEMS suspended part highlighting its layered structure: the PEN substrate (25  $\mu\text{m}$ ) is covered with a piezoelectric PVDF-TrFE layer (4  $\mu\text{m}$ ) sandwiched between two aluminum electrodes (100 nm). A protective PDMS layer (6  $\mu\text{m}$ ) is deposited on the top of the structure and covered with the switchable magnetic molecule (<500 nm). **(d)** Temperature dependence of the resonance frequency,  $f_0$ , of the pristine structure. The stiffness of the resonator increases with decreasing temperature leading to an increase of the resonance frequency when lowering the temperature. Inset: a typical resonance spectrum of the well-compensated piezoelectric resonator. **(e)** SEM micrograph of the molecule-based MEMS with the functionalized area in purple that contrasts with the uncovered area in green (artificially colored view). Scale bar is 100  $\mu\text{m}$ . Inset: molecular structure of complex SCO1, that exhibits spin-crossover (SCO) properties.

Moreover, the present results have been reproduced with different molecular systems under different forms, thus demonstrating the versatility of our approach.

The piezoelectric MEMS used in this work are organic and fabricated at low-cost thanks to a rapid and simple process (Methods)<sup>20</sup>. They are made of a multilayer assembly consisting of a polyethylene naphthalate (PEN) substrate covered with the piezoelectric copolymer, poly(vinylidene fluoride-trifluoroethylene) (PVDF-TrFE), sandwiched between two thin layers of aluminum<sup>20</sup> (Fig. 1b,c). Thanks to the polymer piezoelectricity, the resonators are actuated by applying a voltage across the two parallel aluminum electrodes. The detection of the mechanical resonance is achieved by measuring the change of the motional impedance,  $Z_m$ , of the piezoelectric layer, induced by the displacement (Methods). Prior to the functionalization of the MEMS with MMSs, the temperature dependence of the first flexural mode,  $f_0$ , was investigated. For this purpose, the MEMS device was cooled down using a liquid nitrogen cryostat and the resonance curves were collected for different temperatures (Fig. 1d). The characteristic frequency  $f_0$  exhibits a quadratic behavior mainly due to the dependence of the Young's modulus with temperature. A significant change of  $f_0$  was not observed during the different thermal cycling. In addition, it should be mentioned that at low temperatures, around liquid nitrogen temperature, some frequency instability have been observed, probably due to the freezing out of the charges in the piezoelectric material, however, as soon as the devices reaches 90 K this instability vanishes.

To demonstrate the feasibility of our detection method, we focused first on the  $[\text{Fe}(\text{dmbpy})(\text{H}_2\text{B}(\text{pz})_2)_2]$  spin crossover compound (noted SCO1; dmbpy = 4,4'-dimethyl-2,2'-bipyridine and  $\text{H}_2\text{B}(\text{pz})_2$  = dihydrobis(pyrazolyl) borate; Figs 1e and S1), as it exhibits a large change of unit cell volume (6%) at the crossover temperature (See supporting information). SCO1 was either dissolved in methanol and dropcasted onto the MEMS surface (device A; Fig. 1e), or directly sublimated using a thermal evaporator (device B), as reported in reference<sup>21</sup>. Figure 2a shows the resonance frequency for device A as a function of the temperature for pristine and hybrid resonators. A clear decrease of  $f_0$  is observed around 165 K for the hybrid resonator, which corresponds to the spin crossover temperature measured by standard magnetometry on bulk samples (Fig. S2). It is important to note, that this behavior is reproducible upon thermal cycling. To highlight the effect of the spin crossover on the mechanical response, we apply a quadratic correction to  $f_0$  which suppresses the intrinsic temperature dependence of the resonator structure. The Fig. 2b presents the evolution of  $\Delta f^*/f^*$ , the relative variation of the corrected frequency that is directly compared to the signature of the spin crossover phenomenon obtained by direct magnetic measurements (Fig. 2c,d for devices A and B, respectively). These results prove that the large variations of the organic MEMS resonance frequency are induced by the spin crossover phenomenon of the molecules. Moreover, it clearly indicates that the deposition method does not strongly affect the crossover.

The shift of the resonance frequency is the consequence of a mechanical alteration of the resonator triggered by the switchable molecules at the spin crossover temperature. Two main effects have been discussed in the literature<sup>15,18,19</sup>: (i) the change of mechanical properties of the material (Young's modulus, mass density) and (ii)

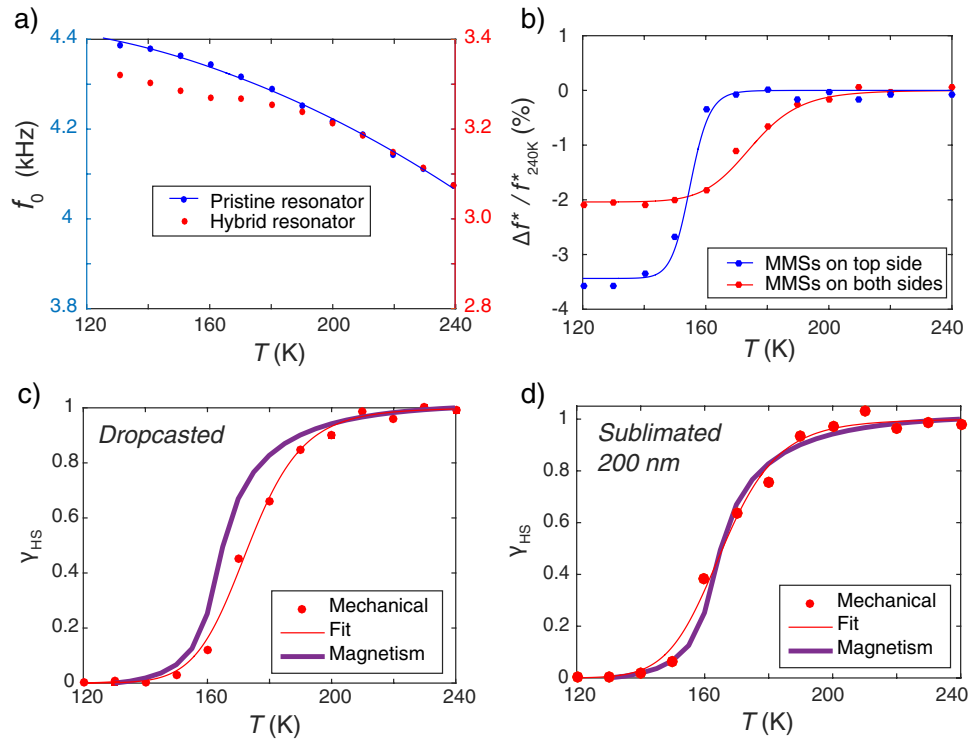


**Figure 2.** Molecule-based MEMS and detection of the spin crossover phenomenon. (a) Comparison of the resonance frequency as a function of temperature before and after functionalization of the resonator (here as an illustrating example with **SCO1** molecules). The hybrid resonator shows a drop of the resonance frequency around 165 K. (b) Relative variation of the resonance frequency corrected with the quadratic behavior of the pristine resonator. The red (blue) curve corresponds to a single (double)-side functionalization by MMSs (dropcasted). (c,d) High spin fraction of the **SCO1** molecules as a function of the temperature. The red dots are extracted from the mechanical response (resonance frequency) of the resonator functionalized with dropcasted (c; Device A; frequency data are shown in Fig. 2a) or sublimated (d; Device B) MMSs. The experimental data are then fitted using a Fermi distribution (continuous line). The purple curve corresponds to magnetometry measurement performed on a polycrystalline sample of **SCO1** using a SQUID magnetometer (See Fig. S2).

the change of surface stress at the interface between MMSs and the resonator. The total relative frequency shift,  $[\Delta f_0/f_0]^{Total}$ , is thus given by Equation 1:

$$\left[ \frac{\Delta f_0}{f_0} \right]^{Total} = \left[ \frac{\Delta f_0}{f_0} \right]^{Material} + \left[ \frac{\Delta f_0}{f_0} \right]^{Stress} \quad (1)$$

The relative frequency shift due to mechanical properties,  $[\Delta f_0/f_0]^{Material}$ , was discussed in ref.<sup>19</sup>. Applying this model to our devices gives a theoretical  $[\Delta f_0/f_0]^{Material}$  value of +0.16% (See supporting information). This estimation is clearly contrasting with our results, which reveal a total shift of -2.25% (Fig. 2b). The detected resonance shift is thus dominated by the surface stress that implies two contributions<sup>19</sup>: (i) the differential surface stress,  $\sigma_s^{Diff} = \sigma_s^{Upper} - \sigma_s^{Lower}$  (with  $\sigma_s^{Upper}$  and  $\sigma_s^{Lower}$ , the surface stresses applied to the upper and lower faces of the cantilever) that induces a bending of the cantilever and (ii) the total surface stress:  $\sigma_s^{Total} = \sigma_s^{Upper} + \sigma_s^{Lower}$ . While the first component is known to have a negligible effect on the resonance frequency<sup>22</sup>, the total surface stress strongly influences the cantilever resonance frequency<sup>23</sup>. The analytical expression of  $[\Delta f_0/f_0]^{Stress}$  in relation with the total surface stress is explicitly given by Lachut and Sader<sup>23</sup>, Equation 2:

$$\left[ \frac{\Delta f_0}{f_0} \right]^{Stress} = -0.042 \frac{\nu(1-\nu)\sigma_s^{Total}}{Eh} \left( \frac{b}{L} \right) \left( \frac{b}{h} \right)^2 \quad (2)$$

with  $L$  being the cantilever length,  $b$  the width,  $h$  the thickness,  $E$  the equivalent Young's modulus of the multi-stacked device, and  $\nu$  the Poisson ratio. Applying this approach to our hybrid MMS/MEMS resonators gives a stress induced in the MMSs material of 250 MPa  $\left( \sigma_{MMS} = \frac{\sigma_s^{Total}}{\nu_{MMS}} \right)$  for an experimental resonance frequency shift of -2.25%. To further demonstrate the key role of the total surface stress on the resonance frequency, the resonator was functionalized with MMSs on both its top and bottom faces as a significant increase of the shift is expected, whereas an effect of the differential surface stress should cancel this shift. As shown in Fig. 2b,  $[\Delta f_0/f_0]^{Total}$  indeed

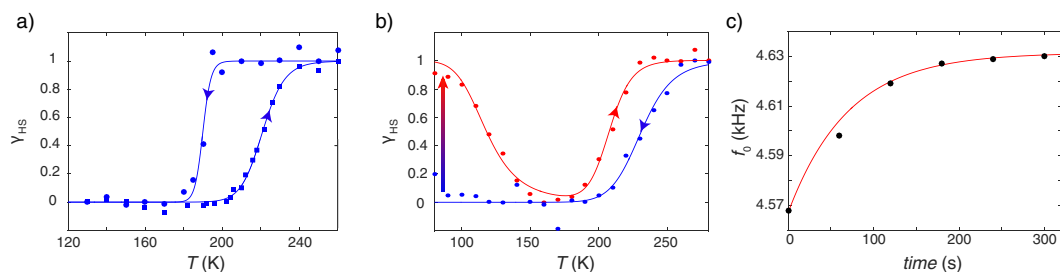


**Figure 3.** Bistable molecule-based MEMS. **(a)** High spin fraction of **SCO2** molecules as a function of the temperature. The blue dots and squares are deduced from the experimental mechanical response (resonance frequency) of the organic resonator functionalized with dropcasted MMSs in cooling and heating modes, respectively. The continuous lines are guides for the eyes. The first order phase transition of the deposited molecule-based material induces a thermal hysteric effect giving rise to a bistable behavior. **(b)** High spin fraction of **ET3** molecules as a function of the temperature. The blue and red dots are deduced from the experimental mechanical response (resonance frequency) of the organic resonator functionalized with dropcasted MMSs in cooling (in the dark) and heating (in the dark after light irradiation at 80 K) modes, respectively. The continuous lines are guides for the eyes. **(c)** Time evolution of the resonance frequency of the organic MEMS functionalized with **ET3** during illumination at 80 K with white light ( $P = 1 \text{ mW/cm}^2$ ).

increases to  $-3.8\%$ , in agreement with the prediction of our model. It is also possible to compare the surface stress value,  $\sigma_{MMS}$ , of 250 MPa obtained with the above model with the stress,  $\sigma_{MMS}^* = \varepsilon_{MMS}^* E_{MMS} / (1 - \nu_{MMS})$ , that should be induced by eigenstrain due to MMS volume change ( $\varepsilon_{MMS}^* = \frac{1}{3} \Delta V / V$ ). The numerical estimation of  $\sigma_{MMS}^*$  leads to 145 MPa, which is in relative good agreement with the  $\sigma_{MMS}$  value obtained above, especially considering that  $\sigma_{MMS}^*$  does not take into account effects at the interface between MMSs and the MEMS resonator. The present analysis establishes that the origin of the frequency shift observed is the total surface stress induced by the volume change of the switchable molecules. This work also underlines the benefits for molecular sensing using MMSs when combined with organic MEMS. Their low Young's modulus leads to highly sensitive sensors with large frequency shift responses. It is interesting to note that there is a slight difference in the characteristic spin crossover temperature between the two curves in Fig. 2b (140 K and 160 K). This effect can be explained considering that the molecules, which are deposited on the top layer, can move freely, meaning that at the spin crossover, the stress induced by the reduction of volume is released thanks to the bending of the MEMS. In this case, the mechanical curve reproduces the same thermal behaviour as the magnetization data observed for a polycrystalline sample. When both MEMS sides are covered, it becomes more difficult for the stress to be released and as a result, it requires more energy for the molecules to overcome the spin-crossover and thus the associated temperature is modified.

In order to test the versatility of our molecule-based sensors, **SCO1** has been replaced by another switchable complex:  $\text{Fe}(\text{MeOL-mCl})_2$  (noted **SCO2**; MeOL-mCl:  $\text{N}'((5\text{-chloropyridin-2-yl)methylene})\text{-4-methoxybenzohydrazonate}$ ; Fig. S3; see supporting information). This compound exhibits a magnetic change from HS to LS through a first order phase transition induced by strong elastic interactions between molecules. As a consequence, at finite temperature sweep rate, a thermal hysteresis is observed (see Fig. S4), which could confer our sensor a memory effect. As for device A, **SCO2** has been dropcasted onto the organic MEMS. From the temperature dependence of  $f_0$ , before and after deposition, the HS fraction of **SCO2** was estimated for a thermal cycle between 300 and 120 K (a cooling/warming cycle). As shown in Fig. 3a, the spin crossover is preserved after deposition of **SCO2** and as expected for a spin transition, it appears more abrupt than for devices A and B coated with **SCO1**. The presence of a thermal hysteresis loop between 220 and 180 K, larger than in the **SCO2** bulk material (Fig. S4), is clearly observed. This reveals that the elastic interactions in this material are still active and even reinforced after the deposition. It is worth mentioning, that in contrast with **SCO1** where the intermolecular interactions are much weaker, the switching process is instantaneous and discontinuous (as expected for a 1<sup>st</sup> order phase transition), inducing an abrupt change in the mechanical properties, which are thus not fully reversible. As a consequence, the life time of such bistable device is limited to only few thermal cycles. A better control of the elastic interactions between the molecules should allow us to study and control the fundamental physics underlying such switching processes. However, at this stage, the present result opens perspectives toward the use of spin transition materials in molecule-based sensors exhibiting non-volatile memory.

Another interesting property of some MMSs is their ability to be photo-switched between their different magnetic states. To probe the possibility to build photo-active sensors, an electron transfer molecule, ( $\{(\text{pzTp})\text{Fe}(\text{CN})_3\}_4[\text{Co}(\text{pz})_3\text{CCH}_2\text{OH}]_4[\text{ClO}_4]_4\} \cdot 13\text{DMF} \cdot 4\text{H}_2\text{O}$  noted **ET3**; pzTp = tetrakis(pyrazolyl)borate and  $(\text{pz})_3\text{C-CH}_2\text{OH} = 2,2,2\text{-tris}(1\text{-pyrazolyl})\text{ethanol}$ ; see supporting information) has been considered in this study as it can be photoswitched at liquid nitrogen temperature<sup>24</sup>. These molecules have been directly dropcasted onto the organic MEMS. The high-spin fraction of **ET3** was estimated from  $f_0$  upon decreasing the temperature from 300 to 80 K as shown by the blue symbols in Fig. 3b. A magnetic switching of the **ET3** molecules from the HS to the LS states is observed around 230 K. This magnetic conversion seems to be less abrupt than in the original **ET3** material<sup>24</sup> and slightly shifted of about 20 K to lower temperatures. At 80 K, the **ET3**-based hybrid device was irradiated with white light while the time evolution of  $f_0$  was recorded (Fig. 3c). In less than 5 minutes,  $f_0$  increases from 4.57 kHz to a saturation value of 4.63 kHz. It is important to note that the dynamical evolution under illumination

depends on the light intensity. To avoid any parasitic light-induced heating, we have worked at relatively low irradiation power ( $P = 1 \text{ mW/cm}^2$ ). The HS fraction estimated from this  $f_0$  variation evidences the complete photo-conversion of the ET3 molecules at 80 K (Fig. 3b). When increasing the temperature in the dark (the red symbols in Fig. 3b), the hybrid MEMS recovers the resonance frequency as before irradiation at 150 K. This feature, also seen in the original ET3 material at about 200 K, corresponds to the relaxation of the photo-induced HS molecules into their LS ground state; in other words, the system at 150 K has enough thermal energy to overcome the barrier separating the metastable and thermodynamic states. Further increase of the temperature leads to a recovery of the HS state above 220 K (Fig. 3b). It is worth noting that the difference between the cooling and warming branches contrasts with the absence of thermal hysteresis in the bulk ET3 material. This observation and the fact that the characteristic relaxation temperature of the photo-induced state is different for the hybrid device (150 K) and the original ET3 compound (200 K) strongly suggests that the ET3 molecules do not organize on the surface of the resonator with the same interaction pattern as in the bulk material. Consequently, this type of device could be very interesting to investigate the switchable properties of molecules in thin films. This last example highlights the remarkable versatility of these molecule-based microelectromechanical sensors: they can be triggered by temperature, as observed for the three reported hybrid devices, but also by light at a fixed temperature when functionalized with ET3 molecules.

Combining organic MEMS with switchable magnetic molecules has allowed us to detect large variations of the resonance frequency induced by a small change of volume at the molecular scale. Providing that this class of switchable molecules is extremely sensitive to external stimuli (such as temperature, light, pressure, chemical atmosphere...), these hybrid devices are promising systems for sensing applications<sup>9–18</sup>. In this work, we have indeed demonstrated that the reported molecule-based MEMS could be operated as a temperature and light detector as well as a non-volatile memory. These results pave the way toward an integration of organic MEMS devices in molecular electronics.

## Methods

**Fabrication of devices.** The fabrication process starts with a 25  $\mu\text{m}$  thick PEN film, used as a substrate, cleaned with isopropanol. Then, 300 nm of aluminum is evaporated through a PET (polyethylene terephthalate) shadow mask to pattern the bottom electrodes (for the free-standing cantilever and the reference capacitance). The deposition of the PVDF-TrFE layer is then achieved by using PVDF-TrFE powder (75–25% in mole; Piezotech) dissolved in 2-butanone with a mass content of 20%. This solution is spin-coated at 3500 rpm with a ramp of 1 second for 45 seconds, giving a thickness of about 4  $\mu\text{m}$ . The resulting assembly is then annealed at 50 °C for 10 minutes to evaporate the solvent and at 140 °C for a hour to improve crystallinity. The aluminum top electrode is subsequently evaporated in the same conditions as the bottom one through a PET shadow mask. A 6  $\mu\text{m}$  protective PDMS (polydimethylsiloxane; Sylgard 184, Dow Corning) layer is spin-coated on the top surface of the devices and cured at 80 °C for 2 hours. To finish the assembly process, the shape of the cantilever is obtained simply by xurography, thanks to a vinyl cutting machine Craft RoboPro CE6000 (Graftec Craft ROBO Pro). For proper use, the resulting MEMS resonators are glued on a glass blade with a double-sided adhesive tape, leaving the cantilever part suspended and the reference capacitance fixed. To induce piezoelectricity in the PVDF-TrFE film, the set-up is poled with a DC electric field of 100 V/ $\mu\text{m}$  for 10 minutes. It is worth mentioning that the obtained MEMS devices possess quality factors between 15 and 35.

**Device measurement.** The total impedance  $Z_t$  between the two aluminum electrodes is composed of the motional impedance  $Z_m$  with a constant capacitance  $C_0$  in parallel ( $C_0$  corresponds to the geometrical capacitor made of the PVDF-TrFE dielectric layer sandwiched between the two aluminum electrodes). To measure directly the variation of  $Z_m$ , a reference capacitance  $C_0$  has been integrated on the MEMS chip, see Fig. 1b. It is composed of the same stacked layers but not free to move. An alternative signal is then applied on both structures with an independent, tunable amplitude of opposite sign to compensate the effect of  $C_0$ . The voltage at the common electrode is then zero except when the free structure starts to move. Both the amplitude and phase are obtained using an IQ demodulator and then the resonance frequency  $f_0$  can easily be measured by a dedicated electronic card. The measurement error is less than few Hz on the resonance frequency (in the experimental kHz range) and less than 0.5 K over the 80–300 K range using an optical cryostat.

## References

- Liu, S. F., Petty, A. R., Sazama, G. T. & Swager, T. M. Single-Walled Carbon Nanotube/Metalloporphyrin Composites for the Chemiresistive Detection of Amines and Meat Spoilage. *Angew. Chemie Int. Ed.* **54**, 6554–6557 (2015).
- Kim, H.-U. *et al.* A sensitive electrochemical sensor for *in vitro* detection of parathyroid hormone based on a MoS<sub>2</sub>-graphene composite. *Sci. Rep.* **6**, 34587 (2016).
- Hu, H. *et al.* Far-field nanoscale infrared spectroscopy of vibrational fingerprints of molecules with graphene plasmons. *Nat. Commun.* **7**, 12334 (2016).
- Kulkarni, G. S., Reddy, K., Zhong, Z. & Fan, X. Graphene nanoelectronic heterodyne sensor for rapid and sensitive vapour detection. *Nat. Commun.* **5**, 4376 (2014).
- Jia, C. *et al.* Covalently bonded single-molecule junctions with stable and reversible photoswitched conductivity. *Science*. **352**, 1443–1446 (2016).
- Fu, Y. S. *et al.* Reversible chiral switching of bis(phthalocyaninato) Terbium(III) on a metal surface. *Nano Lett.* **12**, 3931–3935 (2012).
- Hieringer, W. *et al.* The Surface Trans Effect: Influence of Axial Ligands on the Surface Chemical Bonds of Adsorbed Metalloporphyrins. *J. Am. Chem. Soc.* **133**, 6206–6222 (2011).
- Weigelt, S. *et al.* Chiral switching by spontaneous conformational change in adsorbed organic molecules. *Nat. Mater.* **5**, 112–117 (2006).
- Bousseksou, A., Molnar, G., Salmon, L. & Nicolazzi, W. Molecular spin crossover phenomenon: recent achievements and prospects. *Chem. Soc. Rev.* **40**, 3313–3335 (2011).
- Gutlich, P., Hauser, A. & Spiering, H. Thermal and Optical Switching of Iron(II) Complexes. *Angew. Chemie Int. Ed. English* **33**, 2024–2054 (1994).

11. Matsumoto, T. *et al.* Programmable spin-state switching in a mixed-valence spin-crossover iron grid. *Nat. Commun.* **5**, 3865 (2014).
12. Hayami, S., Holmes, S. M. & Halcrow, M. A. Spin-state switches in molecular materials chemistry. *J. Mater. Chem. C* **3**, 7775–7778 (2015).
13. Aguilà, D., Prado, Y., Koumoussi, E. S., Mathonière, C. & Clérac, R. Switchable Fe/Co Prussian blue networks and molecular analogues. *Chem. Soc. Rev.* **45**, 203–224 (2016).
14. Koumoussi, E. S. *et al.* Metal-to-Metal Electron Transfer in Co/Fe Prussian Blue Molecular Analogues: The Ultimate Miniaturization. *J. Am. Chem. Soc.* **136**, 15461–15464 (2014).
15. Shepherd, H. J. *et al.* Molecular actuators driven by cooperative spin-state switching. *Nat. Commun.* **4**, 3607 (2013).
16. Manrique-Juárez, M. D. *et al.* Switchable molecule-based materials for micro- and nanoscale actuating applications: Achievements and prospects. *Coord. Chem. Rev.* **308**, 395 (2015).
17. Gural'skiy, I. A. *et al.* Spin crossover composite materials for electrothermomechanical actuators. *J. Mater. Chem. C* **2**, 2949 (2014).
18. Manrique-Juarez, M. D. *et al.* A Bistable Microelectromechanical System Actuated by Spin-CrossoverMolecules. *Angew. Chemie Int. Ed.* **56**, 8074–8078 (2017).
19. Maria D. Manrique-Juarez, *et al.* Microelectromechanical systems integrating molecular spin crossover actuators. *Applied Physics Letters* **109**(6), 061903 (2016).
20. Ducrot, P.-H., Dufour, I. & Ayela, C. Optimization of PVDF-TrFE processing conditions for the fabrication of organic MEMS resonators. *Sci. Rep.* **6**, 19426 (2016).
21. Shi, S. *et al.* Study of molecular spin-crossover complex Fe(phen)<sub>2</sub>(NCS)<sub>2</sub> thin films. *Appl. Phys. Lett.* **95**, 43303 (2009).
22. Sader, J. E. Surface stress induced deflections of cantilever plates with applications to the atomic force microscope: V-shaped plates. *J. Appl. Phys.* **91**, 9354–9361 (2002).
23. Lachut, M. J. & Sader, J. E. Effect of Surface Stress on the Stiffness of Cantilever Plates. *Phys. Rev. Lett.* **99**, 206102 (2007).
24. Li, D. *et al.* Magnetic and Optical Bistability Driven by Thermally and Photoinduced Intramolecular Electron Transfer in a Molecular Cobalt - Iron Prussian Blue Analogue. *J. Am. Chem. Soc.* **130**, 252–258 (2008).

## Acknowledgements

This study has been carried out with financial support from the Institut de Chimie of the Centre National de la Recherche Scientifique (CNRS), the Université de Bordeaux, the Région Nouvelle Aquitaine, the GDR MCM2, the MOLSPIN COST action CA15128 the Agence Nationale de la Recherche (ANR; N°ANR-13-PDOC-0032) and the LabEx AMADEus (ANR-10-LABX-42) in the framework of IdEx Bordeaux (ANR-10-IDEX-03-02), that is, the Investissements d'Avenir programme of the French government managed by the ANR. We also thank M. Abbas and L. Hirsch for experimental support, and J.F. Tassin who has encouraged us to develop this project and has facilitated the short stay of M.U. at the Centre de Recherche Paul Pascal.

## Author Contributions

M.U., C.A. and R.C. initiated the project and designed the experiments. P.-H.D. and C.A. fabricated the MEMS devices. D.R.A., A.M., C.M., P.D. and R.C. synthesized and characterized the MMSs. F.M. conceived the electronic board for the MEMS excitation and data acquisition. The experiments were carried out by M.U., M.R. and C.A.; I.D. and C.A. developed the model. All authors discussed the results. M.U., R.C. and C.A. wrote the manuscript with inputs from all authors.

## Additional Information

**Supplementary information** accompanies this paper at <https://doi.org/10.1038/s41598-018-26076-2>.

**Competing Interests:** The authors declare no competing interests.

**Publisher's note:** Springer Nature remains neutral with regard to jurisdictional claims in published maps and institutional affiliations.



**Open Access** This article is licensed under a Creative Commons Attribution 4.0 International License, which permits use, sharing, adaptation, distribution and reproduction in any medium or format, as long as you give appropriate credit to the original author(s) and the source, provide a link to the Creative Commons license, and indicate if changes were made. The images or other third party material in this article are included in the article's Creative Commons license, unless indicated otherwise in a credit line to the material. If material is not included in the article's Creative Commons license and your intended use is not permitted by statutory regulation or exceeds the permitted use, you will need to obtain permission directly from the copyright holder. To view a copy of this license, visit <http://creativecommons.org/licenses/by/4.0/>.

© The Author(s) 2018